REPORT DOCUMENTATION PAGE

Form Approved
OMB No. 0704-0188

1. REPORT DATE *(DD-MM-YYYY)*	**2. REPORT TYPE**	**3. DATES COVERED** *(From - To)*
2011	Open Literature – Journal Article	

4. TITLE AND SUBTITLE
Role of acetylcholinesterase on the structure and function of cholinergic synapses: insights gained from studies on knockout mice

5a. CONTRACT NUMBER

5b. GRANT NUMBER

5c. PROGRAM ELEMENT NUMBER

6. AUTHOR(S)
Adler, M, Sweeney, R., Hamilton, TA, Lockridge, O, Duysen, EG, Purcell, AL, Desphpande, SS

5d. PROJECT NUMBER

5e. TASK NUMBER

5f. WORK UNIT NUMBER

7. PERFORMING ORGANIZATION NAME(S) AND ADDRESS(ES)

US Army Medical Research Institute of Chemical Defense
ATTN: MCMR-CDT-N
3100 Ricketts Point Road
Aberdeen Proving Ground, MD 21010-5400

8. PERFORMING ORGANIZATION REPORT NUMBER

USAMRICD-P11-022

9. SPONSORING / MONITORING AGENCY NAME(S) AND ADDRESS(ES)

US Army Medical Research Institute of Chemical Defense
ATTN: MCMR-CDZ-I
3100 Ricketts Point Road
Aberdeen Proving Ground, MD 21010-5400

10. SPONSOR/MONITOR'S ACRONYM(S)

11. SPONSOR/MONITOR'S REPORT NUMBER(S)

12. DISTRIBUTION / AVAILABILITY STATEMENT

Approved for public release; distribution unlimited

13. SUPPLEMENTARY NOTES

Published in **Cellular and Molecular Neurobiology, 31(6), 909-920, 2011**.This research was supported by the Defense Threat Reduction Agency-Joint Science and Technology Office, Medical S & T Division.

14. ABSTRACT

See reprint.

15. SUBJECT TERMS

Neuromuscular junction , Cholinesterase, Knockout mouse, Diaphragm muscle, Electron microscopy, Endplate potential, Medical chemical defense

16. SECURITY CLASSIFICATION OF:			**17. LIMITATION OF ABSTRACT**	**18. NUMBER OF PAGES**	**19a. NAME OF RESPONSIBLE PERSON**
a. REPORT	**b. ABSTRACT**	**c. THIS PAGE**			Michael Adler
UNCLASSIFIED	UNCLASSIFIED	UNCLASSIFIED	UNLIMITED	12	**19b. TELEPHONE NUMBER** *(include area code)* 410-436-1913

Cell Mol Neurobiol (2011) 31:909–920
DOI 10.1007/s10571-011-9690-5

ORIGINAL PAPER

Role of Acetylcholinesterase on the Structure and Function of Cholinergic Synapses: Insights Gained from Studies on Knockout Mice

Michael Adler · Richard E. Sweeney · Tracey A. Hamilton · Oksana Lockridge · Ellen G. Duysen · Angela L. Purcell · Sharad S. Deshpande

Received: 3 February 2011 / Accepted: 6 April 2011 / Published online: 3 May 2011

Abstract Electrophysiological and ultrastructural studies were performed on phrenic nerve-hemidiaphragm preparations isolated from wild-type and acetylcholinesterase (AChE) knockout (KO) mice to determine the compensatory mechanisms manifested by the neuromuscular junction to excess acetylcholine (ACh). The diaphragm was selected since it is the primary muscle of respiration, and it must adapt to allow for survival of the organism in the absence of AChE. Nerve-elicited muscle contractions, miniature endplate potentials (MEPPs) and evoked endplate potentials (EPPs) were recorded by conventional electrophysiological techniques from phrenic nerve-hemidiaphragm preparations isolated from 1.5- to 2-month-old wild-type ($AChE^{+/+}$) or AChE KO ($AChE^{-/-}$) mice. These recordings were chosen to provide a comprehensive assessment of functional alterations of the diaphragm muscle resulting from the absence of AChE. Tension measurements from $AChE^{-/-}$ mice revealed that the amplitude of twitch tensions was potentiated, but tetanic tensions underwent a use-dependent decline at frequencies below 70 Hz and above 100 Hz. MEPPs recorded from hemidiaphragms of $AChE^{-/-}$ mice showed a reduction in frequency and a prolongation in decay (37%) but no change in amplitude compared to values observed in age-matched wild-type littermates. In contrast, MEPPs recorded from hemidiaphragms of wild-type mice that were exposed for 30 min to the selective AChE inhibitor 5-bis(4-allyldimethyl-ammoniumphenyl)pentane-3-one (BW284C51) exhibited a pronounced increase in amplitude (42%) and a more marked prolongation in decay (76%). The difference between MEPP amplitudes and decays in $AChE^{-/-}$ hemidiaphragms and in wild-type hemidiaphragms treated with BW284C51 represents effective adaptation by the former to a high ACh environment. Electron microscopic examination revealed that diaphragm muscles of $AChE^{-/-}$ mice had smaller nerve terminals and diminished pre- and post-synaptic surface contacts relative to neuromuscular junctions of $AChE^{+/+}$ mice. The morphological changes are suggested to account, in part, for the ability of muscle from $AChE^{-/-}$ mice to function in the complete absence of AChE.

Keywords Neuromuscular junction · Cholinesterase · Knockout mouse · Diaphragm muscle · Electron microscopy · Endplate potential

Abbreviations

ACh	Acetylcholine
AChE	Acetylcholinesterase
AChR	Acetylcholine receptor

M. Adler (✉) · A. L. Purcell · S. S. Deshpande
Neurobehavioral Toxicology Branch, Analytical Toxicology Division, US Army Medical Research Institute of Chemical Defense, Aberdeen Proving Ground, MD 21010-5400, USA
e-mail: michael.adler2@us.army.mil

R. E. Sweeney
Pharmacology Branch, Research Division, US Army Medical Research Institute of Chemical Defense, Aberdeen Proving Ground, MD 21010-5400, USA

T. A. Hamilton
Comparative Pathology Branch, Research Support Division, US Army Medical Research Institute of Chemical Defense, Aberdeen Proving Ground, MD 21010-5400, USA

O. Lockridge · E. G. Duysen
Eppley Institute, University of Nebraska Medical Center, Omaha, NE 68198-6805, USA

Present Address:
A. L. Purcell
Cooley LLP, Washington, DC 20001, USA

$AChE^{+/+}$	129SVJ wild-type mice
$AChE^{-/-}$	AChE knockout mice
BChE	Butyrylcholinesterase
BW284C51	1,5-Bis(4-allyldimethyl-ammoniumphenyl)pentane-3-one)
μ-CTX	μ-Conotoxin GIIIB
EPP	Endplate potential
iso-OMPA	Tetraisopropylpyrophosphoramine
KO	Knockout
MEPP	Miniature endplate potential
m_0	Quantal content of the EPP by the method of failure
m_r	Quantal content of the EPP by ratio of EPP/MEPP in μ-conotoxin GIIIB
PBS	Phosphate-buffered saline
SSV	Small synaptic vesicle
TEM	Transmission electron microscopy

Introduction

Neuromuscular transmission is initiated by depolarization of the motoneuron nerve terminal and culminates in the synchronous release of acetylcholine (ACh) from small synaptic vesicles (SSVs) docked at active zones (Heuser et al. 1979). ACh then diffuses across the synaptic cleft and combines with binding sites on two α subunits of the pentameric nicotinic ACh receptor (AChR), leading to the opening of the associated ligand-gated ion channel (Karlin 2002). Channel opening triggers, in turn, the endplate current, endplate potential (EPP), muscle action potential and muscle contraction (Miyazawa et al. 2003). Normal operation of the neuromuscular junction requires removal of ACh within several milliseconds of receptor activation to allow for sustained high frequency firing: otherwise persistence of ACh would lead to membrane depolarization, retrograde firing, receptor desensitization, muscle fasciculation and muscle weakness (Katz and Miledi 1973; Heffron and Hobbiger 1979; Magleby and Pallotta 1981; Adler et al. 1992). Removal of ACh is accomplished primarily by hydrolysis to choline and acetate, neither of which has appreciable agonist action at the neuromuscular junction (Akk et al. 2005), and to a more limited extent by diffusion of ACh from the synaptic cleft (Katz and Miledi 1973).

There are two enzymes capable of hydrolyzing ACh at cholinergic synapses: acetylcholinesterase (AChE, EC 3.1.1.7) and butyrylcholinesterase (BChE, EC 3.1.1.8). AChE is the primary hydrolytic enzyme and produces rapid cleavage of ACh (Zimmerman and Soreq 2006; Colletier et al. 2006). At the neuromuscular junction, under normal conditions, BChE is thought to have little or no role in hydrolysis of ACh due to its lower K_{cat}, higher K_m, lower density and less favorable localization (Chatonnet and Lockridge 1989; Brimijoin and Koenigsberger 1999). However, BChE has been suggested to participate in the hydrolysis of ACh in other systems, such as airway smooth muscle, that function on a slower time scale (Adler et al. 1991). Moreover, BChE has been reported to play a role in the hydrolysis of ACh in the brain of humans with Alzheimer's disease, where selective loss of AChE may lead to a more dominant role for BChE (Mesulam et al. 2002; Lane et al. 2006).

Much of our information on the role of AChE in synaptic transmission has come from use of selective AChE inhibitors such as 1,5-bis(4-allyldimethyl-ammoniumphenyl)pentane-3-one (BW284C51), huperzine, galantamine, rivastigmine, and fasciculin (Bois et al. 1980; Rosenberry et al. 1999; Albuquerque et al. 2006). While these studies have shed light on the consequences of impaired ACh hydrolysis, interpretation of data is often complicated by incomplete inhibition, imperfect selectivity and unrelated "direct" actions of the inhibitors (Bois et al. 1980; Fiekers 1985; Adler et al. 1991).

An alternative approach is to study neuromuscular transmission in a line of AChE knockout (KO) mice ($AChE^{-/-}$) developed in the laboratory of Dr. Oksana Lockridge (Xie et al. 2000; Li et al. 2000). These mice fail to express AChE, but produce normal levels of both soluble and asymmetric forms of BChE. $AChE^{-/-}$ mice have been found to exhibit low body weight and an exaggerated startle response. In addition they manifest fine motor tremors, pinpoint pupils, circling gait and generalized muscle weakness (Duysen et al. 2001). In spite of these abnormalities, $AChE^{-/-}$ mice have a life expectancy of over 3 months, and some are able to live to adulthood, when maintained on a nutritionally balanced liquid diet (Duysen et al. 2002; Minic et al. 2003). The ability of these mice to survive is remarkable since acute inhibition of AChE leads to death within several minutes. Inhibition of AChE is, in fact, the primary mechanism of toxicity for the highly lethal nerve agents (Taylor 1991).

In a previous study, we found that endplates from $AChE^{-/-}$ mice exhibited a marked reduction of AChRs as revealed by decreased binding of fluorescent α-bungarotoxin (Adler et al. 2004). A decrease in AChR density would have the effect of reducing transmitter accumulation by allowing ACh elimination to approach free diffusion limits (Katz and Miledi 1973; Magleby and Pallotta 1981; Girard et al. 2007). To shed further light on the alterations in neuromuscular structure and function in $AChE^{-/-}$ mice, we studied the consequences of loss of AChE on diaphragmatic tensions, on spontaneous miniature endplate potentials (MEPPs) and nerve-evoked endplate potentials (EPPs), and on synaptic ultrastructure. Repetitive indirect stimulation of diaphragm

muscles from AChE$^{-/-}$ mice led to tetanic fade at frequencies ≤50 and ≥200 Hz but to sustained tension at 70 and 100 Hz. Electrophysiological recordings revealed that the probability of release was not altered in AChE$^{-/-}$ mice under low use conditions, but was reduced transiently following high frequency trains. MEPPs in AChE$^{-/-}$ mice had normal amplitudes and lower frequencies, neither of which is characteristic of acute AChE inhibition (Katz and Miledi 1973). MEPP decays were prolonged, but to a much lower extent than in wild-type mice inhibited acutely by BW284C51. Transmission electron microscopic (TEM) studies indicated extensive synaptic remodeling consisting of reductions in nerve terminal size and of post-junctional surface area. These ultrastructural alterations, in conjunction with a reduced receptor density (Adler et al. 2004; Girard et al. 2007) and maintained BChE activity (Li et al. 2000) may be responsible for the ability of the diaphragm muscle to function in the complete absence of AChE.

Materials and Methods

Animal Preparation

Wild-type 129SVJ mice (AChE$^{+/+}$) and nullizygous AChE$^{-/-}$ mice of either sex were obtained from the University of Nebraska Medical Center and housed at the US Army Medical Research Institute of Chemical Defense under an Association for Assessment and Accreditation of Laboratory Animal Care International (AAALAC) accredited animal care and use program. AChE$^{-/-}$ mice were maintained on Ensure fiber™ (Abbott Laboratories, Columbus, OH, USA) in sterile petri dishes (8 ml/mouse per 24-h period), while AChE$^{+/+}$ mice were provided with commercial rodent ration. Both AChE$^{+/+}$ and AChE$^{-/-}$ mice had access to tap water ad libitum. Animal holding rooms were maintained at 70 ± 2 °F with 50 ± 10% relative humidity using at least 10 complete changes per hour of 100% conditioned fresh air. The mice were on a 12-h light/dark full-spectrum lighting cycle. Mice were euthanized by exposure to excess CO_2, and diaphragms were excised and pinned at resting length in Sylgard™-coated dishes containing oxygenated Krebs-Ringer solution of the following composition (mM): NaCl, 145; KCl, 5.4; $CaCl_2$, 1.8; $MgCl_2$, 1.0; $NaHCO_3$, 15; NaH_2PO_4, 1.0; glucose, 11.0. The solution was bubbled with a gas mixture of 95% O_2 and 5% CO_2 and had a pH of 7.3–7.4. Diaphragm muscles were split at the central tendon to provide 2 hemidiaphragms with independent nerve supply, and they were prepared for tension recordings or microelectrode studies, as appropriate. AChE$^{+/+}$ and AChE$^{-/-}$ mice were 58.7 ± 2.9 and 51.6 ± 3.2 days old and weighed 33.9 ± 2.8 and 19.1 ± 0.81 g, respectively, at the time of euthanasia.

Contractility Measurements

Hemidiaphragms with attached phrenic nerves were mounted in tissue baths at 37°C and immersed in an oxygenated Krebs-Ringer solution. To obtain single twitches, the phrenic nerve was stimulated supramaximally (5–7 V) with 0.2-ms pulses at 0.03 Hz. The response of muscles to repetitive stimulation was probed by eliciting 500-ms long trains at frequencies of 20, 50, 70, 100, 200 and 400 Hz. To avoid neuromuscular fatigue, trains were elicited at a low duty cycle (2 trains per min). Stimuli were delivered with a Grass S88 stimulator (Astro-Med Inc., West Warwick, RI, USA). Muscle twitches were measured with an isometric force transducer (Grass FT03, Astro-Med Inc., West Warwick, RI, USA) and analyzed off-line with pClamp 9.2 software (Molecular Devices, Sunnyvale, CA, USA). Resting tensions were adjusted to 0.5 g to obtain optimal twitch tensions. Parameters measured were peak tension, frequency and 90–10% relaxation time.

Intracellular Microelectrode Techniques

MEPPs and EPPs were recorded at 35–37°C from surface fibers of AChE$^{+/+}$ and AChE$^{-/-}$ hemidiaphragms using standard electrophysiological techniques. Muscle fibers were impaled near endplate regions with borosilicate glass microelectrodes filled with 3 M KCl (15–20 MΩ). Criteria for successful impalement consisted of MEPPs with rise times ≤1 ms and stable resting potentials negative to –60 mV. EPPs were elicited by supramaximal rectangular pulses of 0.1 ms using a Grass S88 stimulator applied to phrenic nerves via suction electrodes.

Quantal content of the EPP was determined under conditions of low probability of release by the method of failures (Del Castillo and Katz 1954) and under conditions of normal probability by determining the ratio of EPPs to MEPPs in the presence of μ-conotoxin GIIIB (μ-CTX) (Plomp et al. 1992). For the former, muscles were superfused with a modified Krebs-Ringer solution in which Mg^{2+} was increased to 8 mM and Ca^{2+} was reduced to 1 mM. This solution reduced the probability of release and allowed the quantal nature of the EPP to be determined according to the expression $m_0 = \ln(N/N_0)$, where N is the total number of stimuli and N_0 is the number of stimuli that fail to produce an evoked response (Del Castillo and Katz 1954). At least 50 MEPPs and 50 EPPs were recorded from each fiber for determining m_0.

To calculate m_r, preparations were bathed in μ-CTX for ≥1 h to suppress muscle action potentials, and full-sized EPPs were recorded at 70 Hz for 1 s; m_r was assessed at the beginning (Initial) and at the end of the train (Final) to ascertain whether a decrease in transmitter release played a role in the decline of tensions during repetitive stimulation.

To calculate $m_{r\ Initial}$, the first EPP during the train was divided by the mean amplitude of MEPPs obtained 1 min prior to the train; $m_{r\ Final}$ was calculated by averaging the last 4 EPPs during the train and dividing these by MEPPs obtained 100 ms following the 1-s stimulus trains. The 100-ms interval was selected to provide conditions where the EPPs had returned to baseline but where desensitization was still close to maximum (Elenes and Auerbach 2002). EPPs were corrected for non-linear summation (McLachlan and Martin 1981), and MEPPs were normalized to a resting potential of −70 mV.

Microelectrode signals were recorded with an Axoclamp-2B amplifier. The output signal was digitized at 10,000 samples/s (Digidata 1332A), and analyzed off-line with pClamp 9.2 software (equipment and software from Molecular Devices, Sunnyvale, CA, USA). The parameters measured were peak amplitude, frequency and 90–10% decay time.

Data Analysis

Data were obtained from 38 to 42 muscle fibers in 8–10 $AChE^{+/+}$ and $AChE^{-/-}$ mice, and are expressed as mean ± SEM. Statistical analysis was performed by ANOVA followed by the Bonferroni Multiple Comparisons Test, or the two-tailed Student's *t*-test, as appropriate (InStat, GraphPad Software Inc., La Jolla, CA, USA). A P value ≤ 0.05 was considered to be statistically significant.

TEM Procedures

Diaphragm muscles were fixed by immersion in buffered 1.6% formaldehyde/2.5% glutaraldehyde at 4°C. After incubation for 24 h, muscles were washed 3 times for 15 min each in 0.1 M Na cacodylate buffer (pH 7.4, 194 mOsm/Kg) and post-fixed for 30 min in buffered 1% osmium tetroxide. Tissues were dehydrated through graded ethanol and bathed in propylene oxide for two 15-min periods. This was followed by addition of Poly/bed 812® resin and propylene oxide at ratios (w/w) of 1:1 and 1:3 for 2 h each and by incubation in pure Poly/bed resin overnight under vacuum. Tissues were flat embedded and polymerized at 60°C for 24 h. Semithin sections were used for preliminary morphological assessment and to select areas of interest for TEM. Ultrathin tissue sections for TEM were collected on copper mesh supporting grids and counterstained using uranyl acetate and lead citrate. Observations were performed using a JEOL 1200EX electron microscope.

Reagents

Poly/Bed 812®, propylene oxide (electron microscopy grade) and sodium cacodylate were from Polysciences Inc., Warrington, PA, USA. Glutaraldehyde, paraformaldehyde, and osmium tetroxide (all TEM grade) were purchased from Electron Microscopy Sciences, Fort Washington, PA. Sylgard™ was obtained from Dow Chemical Co., Midland, MI, USA. BW284C51, iso-OMPA, μ-CTX and all other reagents were from Sigma-Aldrich Corp. (St. Louis, MO, USA).

Results

Contractility Studies

The characteristics of single twitches from isolated hemidiaphragm muscles of $AChE^{+/+}$ and $AChE^{-/-}$ mice are summarized in Table 1. Twitch tensions in muscles from $AChE^{-/-}$ mice had larger amplitudes and slower rise and decay times than those observed in wild-type mice. The larger amplitudes were unexpected, especially in light of the lower body weight and overall weakness of these animals (Duysen et al. 2002). Spontaneous muscle fasciculations, which were commonly observed in the intact animal, were not detected in the isolated $AChE^{-/-}$ hemidiaphragm muscle, suggesting that these responses may require a more complete neuronal circuitry.

The ability of diaphragm muscles from $AChE^{-/-}$ mice to develop and maintain tetanic tension was probed by recording responses to repetitive stimulation of the phrenic nerve at frequencies ranging from 20 to 400 Hz. Muscles from wild-type mice maintained tension at these frequencies with little or no decrement (Fig. 1a). Muscles from $AChE^{-/-}$ mice were able to generate sustained tetanic responses at 70 and 100 Hz, but higher or lower stimulation frequencies led to progressive reductions in muscle tension during the 500-ms trains (Fig. 1b). The maintenance of tetanic tensions at 70 and 100 Hz may be a consequence of the relatively slow time course of twitches in $AChE^{-/-}$ mice (Table 1). The slower time course would allow for more effective summation of tension by enabling tetanic fusion to occur at lower frequencies. This may account in part for the finding that functional adaptation in diaphragm muscle of AChE KO mice was more complete

Table 1 Indirectly elicited single twitches in $AChE^{+/+}$ and $AChE^{-/-}$ mice[a]

Condition	Amplitude (g)	Rise time (ms)	Relaxation (ms)
$AChE^{+/+}$	0.9 ± 0.1	7.7 ± 0.5	17.4 ± 0.6
$AChE^{-/-}$	4.7 ± 0.4[b]	15.9 ± 0.8[b]	24.0 ± 0.9[b]

[a] Data are expressed as mean ± SEM and were obtained from 8–21 $AChE^{+/+}$ and 9–11 $AChE^{-/-}$ mice. Tensions were elicited by supramaximal stimulation of the phrenic nerve (5–7 V, 0.2 ms)

[b] Differs significantly from control $AChE^{+/+}$ values, $P \leq 0.05$

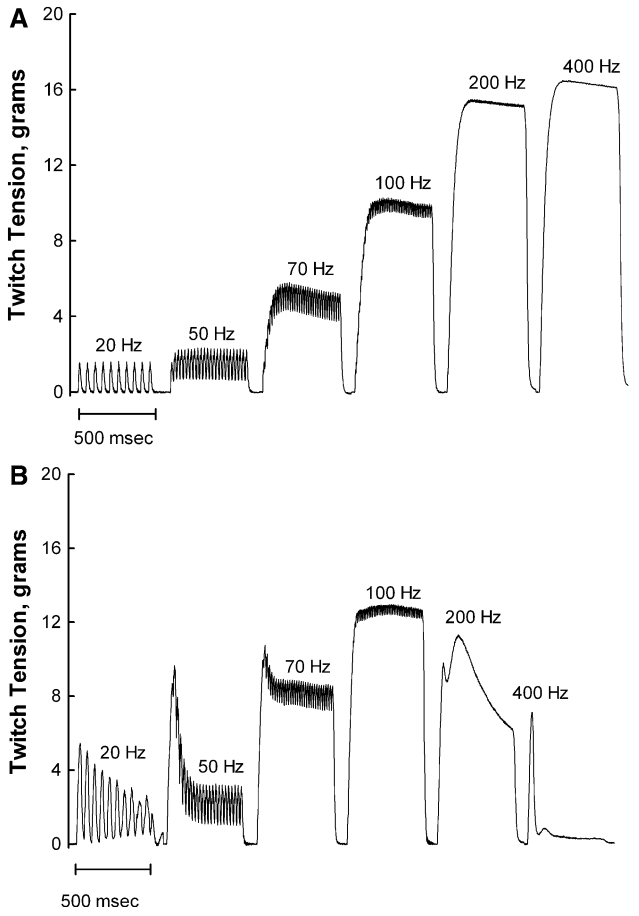

Fig. 1 Muscle tensions in response to repetitive stimulation of the phrenic nerve in AChE$^{+/+}$ (**a**) or AChE$^{-/-}$ (**b**) hemidiaphragms. Tensions were generated by applying 500-ms long stimuli to the phrenic nerve at 20, 50, 70, 100, 200 and 400 Hz. The muscle was allowed to rest for 30 s between stimulus trains. Records were joined at baseline to facilitate presentation. Profiles illustrated are typical of diaphragmatic tensions recorded in muscles isolated from 8–21 AChE$^{+/+}$ and 9–11 AChE$^{-/-}$ mice. Note that at 100 Hz, the tetanus/twich ratio is over 5 in AChE$^{+/+}$ muscle, but only 2.3 in AChE$^{-/-}$ muscle, and that tetanic fusion is achieved at 50 Hz in the latter but only at 70 Hz and above in the former

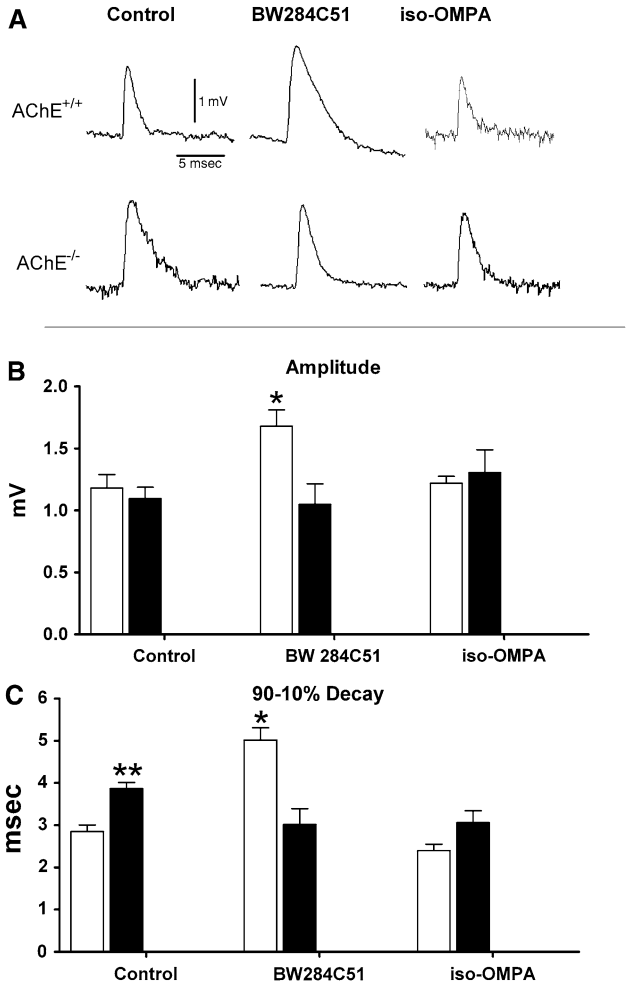

Fig. 2 **a** Traces showing MEPPs recorded from surface fibers of diaphragm muscles under control conditions and 30 min after exposure to the selective AChE inhibitor BW284C51 (1 μM), or the selective BChE inhibitor iso-OMPA (10 μM) in AChE$^{+/+}$ and AChE$^{-/-}$ mice. Note that BW284C1 increased the amplitude and decay of MEPPs in AChE$^{+/+}$ but not in AChE$^{-/-}$ diaphragms, and that iso-OMPA had no effect in either muscle. Calibration bars apply to all traces. **b**, **c** Histograms showing MEPP amplitude and decay in hemidiaphragms from AChE$^{+/+}$ (*open bar*) and AChE$^{-/-}$ (*filled bar*) mice. Values represent the mean ± SEM of 38–42 fibers from 8–10 muscles. *Differs significantly from values in control AChE$^{+/+}$ hemidiaphragm; **Differs significantly from decay in AChE$^{+/+}$ hemidiaphragm, $P < 0.05$. MEPP decays in AChE$^{-/-}$ hemidiaphragms were slightly reduced in BW284C51 and iso-OMPA, but this was not significant by ANOVA

than in the *Tibialis anterior* muscle, where pronounced tetanic fade was observed at frequencies above 50 Hz (Mouisel et al. 2006). Superior adaptation of the diaphragm is consistent with its critical role in the survival of the animal (Nguyen-Huu et al. 2009).

Synaptic Transmission

Representative MEPPs recorded from AChE$^{+/+}$ and AChE$^{-/-}$ mice are shown in Fig. 2a, and quantal responses averaged from 38 to 42 fibers in 8–10 muscles are summarized in Fig. 2b, c. MEPPs represent spontaneous release of ACh from active zones, and their amplitude, frequency and time course reveal important information about alterations of neuromuscular transmission that result from the absence of AChE. MEPPs recorded from hemidiaphragm muscle of AChE$^{+/+}$ mice exhibited an amplitude of 1.18 ± 0.11 mV, a decay time of 2.85 ± 0.16 ms and a frequency of 2.18 ± 0.21/s, which are typical values for control MEPPs in mammalian skeletal muscle (Del Castillo and Katz 1954; Yu and Van der Kloot 1991). MEPPs recorded in hemidiaphragm muscle of AChE$^{-/-}$ mice had an amplitude similar to control (1.09 ± 0.10 mV), but a lower frequency (1.38 ± 0.15/s)

and a longer decay time (3.87 ± 0.14 ms). MEPPs in AChE$^{-/-}$ mice were less severely altered, however, than those of wild-type mice following acute inhibition of AChE. Thus, addition of 1 μM BW284C51 to diaphragm muscles of AChE$^{+/+}$ mice resulted in a 97.8 ± 0.7% inhibition of AChE (Adler et al. 2004), leading to a 76% increase in MEPP decay time and a 42% increase in MEPP amplitude (Fig. 2). Addition of BW284C51 to muscles from AChE$^{-/-}$ mice was without effect, consistent with the absence of AChE in this preparation (Fig. 2).

Since AChE$^{-/-}$ mice are able to express normal levels of BChE (Xie et al. 2000; Li et al. 2000; Minic et al. 2003; Girard et al. 2007), hydrolysis of ACh by BChE may contribute to the maintenance of cholinergic function and thus enable the survival of these animals. To examine this possibility, we recorded MEPPs in the presence of the selective BChE inhibitor iso-OMPA (10 μM). At this concentration, iso-OMPA inhibits 89% of BChE but only 12% of AChE (Adler et al. 2004). If BChE contributes to the hydrolysis of ACh, MEPPs would be expected to show increased amplitudes and prolonged decays in the presence of iso-OMPA. The actions of iso-OMPA would be especially prominent in muscles from AChE$^{-/-}$ mice, where BChE is the only enzyme capable of hydrolyzing ACh. As indicated in Fig. 2, however, iso-OMPA failed to alter MEPP amplitudes or decay times in diaphragm muscle from either AChE$^{-/-}$ or wild-type animals. This is in agreement with the findings of Girard et al. (2007), who saw no effect of 100 μM iso-OMPA on miniature endplate current amplitudes or decays. These results make it unlikely that BChE is responsible for the relatively normal synaptic responses in AChE$^{-/-}$ mice. However, BChE does appear to contribute to the hydrolysis of ACh during repetitive stimulation as evidenced by the finding that iso-OMPA markedly enhanced tetanic fade in hemidiaphragm muscles from AChE$^{-/-}$ mice during high frequency stimulation (≥70 Hz) (Adler et al. 2004). This finding, in conjunction with the report that BChE can hydrolyze ACh in the hippocampus of AChE KO mice (which have high resting levels of ACh), suggests that BChE is effective under conditions where ACh is maintained at a steady high level (Hartmann et al. 2007), but not during the brief time course of a single synaptic event.

To determine whether AChE$^{-/-}$ mice exhibit alterations in evoked release, we examined the quantal content of the EPP under conditions where EPPs are reduced to small multiples of unit responses, as well as under conditions that allow for recording of full-sized EPPs. Figure 3 shows superimposed traces of EPPs from hemidiaphragm muscles of AChE$^{+/+}$ and AChE$^{-/-}$ mice in a high Mg^{2+}/low Ca^{2+} solution, which reduced the probability of release. From the ratio of the number of stimulations/number of failures, it is possible to determine m_0, the mean number of quanta per nerve impulse (Del Castillo and Katz 1954). In AChE$^{+/+}$ mice, m_0 was calculated to be 2.14 ± 0.19 under the present experimental conditions. In muscles from AChE$^{-/-}$ mice, m_0 was determined to be 1.90 ± 0.13, a reduction of only 11%, which was not statistically significant. An absence of change in quantal content was previously reported by Minic et al. (2003) in AChE$^{-/-}$ mice. Further examination of EPPs in diaphragms of AChE$^{-/-}$ and AChE$^{+/+}$ mice revealed that there were no differences in latency (time from nerve stimulation to the onset of response) and in rise time, while the decay of the EPP was prolonged (similar to that of the MEPP). These results suggest that evoked synaptic transmission in diaphragm muscle is well-maintained in AChE$^{-/-}$ mice.

Recordings of EPPs and MEPPs in μ-CTX

To examine neuromuscular transmission under conditions approximating those of the contractility experiments, recordings were made in the presence of 2.5 μM μ-CTX, which selectively inhibits muscle Na^+ channels and allows

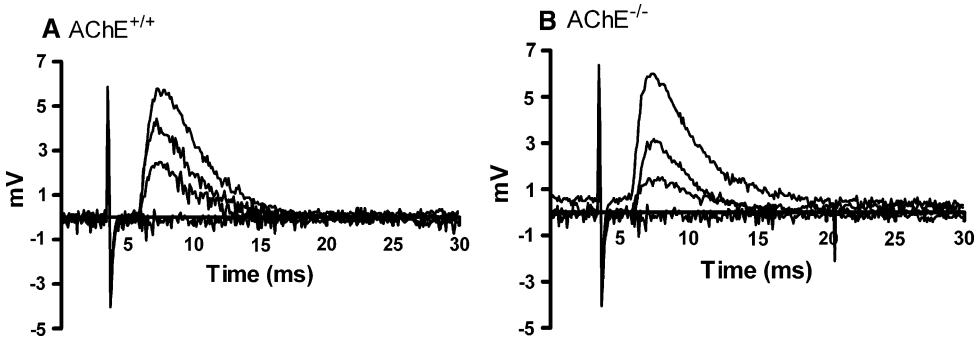

Fig. 3 Superimposed traces showing evoked EPPs recorded from the endplate region of hemidiaphragm muscles isolated from AChE$^{+/+}$ (**a**) and AChE$^{-/-}$ (**b**) mice. EPPs were elicited by supramaximal nerve stimulation at 0.5 Hz in a modified Krebs-Ringer solution containing 8 mM Mg^{2+} and 1 mM Ca^{2+} to suppress muscle action potentials and twitches. Failure of EPP generation is reflected by the horizontal traces lacking responses. Four superimposed traces are shown for each condition. The triphasic responses preceding the EPPs are stimulus artifacts

for the recording of full-sized EPPs. Representative records elicited at 70 Hz in AChE$^{+/+}$ and AChE$^{-/-}$ hemidiaphragms are illustrated in Fig. 4. EPPs in wild-type muscle showed a typical pattern consisting of initial facilitation followed by moderate depression and then a gradual but incomplete recovery for the duration of the train (Moyer and Van Lunteren 1999) (Fig. 4a). Transient depression of EPPs during high frequency stimulation has been ascribed to a depletion of immediately releasable SSVs at the active zone of the presynaptic membrane (Elmqvist and Quastel 1965). The last four EPPs are also displayed on an expanded time base in Fig. 4b, which shows MEPPs of normal amplitude (1.0–1.3 mV) during the last 30 ms of the train and in the immediate post-tetanic period (arrows).

The record from the AChE$^{-/-}$ diaphragm depicts a similar pattern but with two notable differences: EPP amplitudes were considerably more depressed than those from muscles of wild-type mice, and a prominent underlying depolarization was consistently observed, especially during the initial 200 ms of stimulation (Fig. 4c). In spite of the marked frequency-dependent reduction in EPP amplitude, however, these responses were better maintained in muscles of AChE KO mice than in control muscles exposed acutely to AChE inhibitors. For the latter, the amplitudes generally diminish with stimulation without reaching a plateau (Kuba et al. 1974).

At the conclusion of the train, two MEPPs were detectible in the AChE$^{-/-}$ muscle (arrows); the one occurring 100 ms from the end of the last EPP being considerably smaller (0.7 mV) than the one observed 50 ms later (1.6 mV) (Fig. 4d). Low amplitude MEPPs were typically found during and immediately following repetitive stimulation and are likely the result of desensitization of the AChRs from accumulation of ACh during the train. The subsequent increase in MEPP amplitude presumably reflects recovery from desensitization during the ensuing post-train period (Magleby and Pallotta 1981; Elenes and Auerbach 2002).

Histograms of EPPs and MEPPs obtained prior to, during and following 70 Hz trains are shown in Fig. 5. MEPPs recorded in the presence of 2.5 μM μ-CTX prior to stimulation had similar amplitudes to those obtained in control Krebs-Ringer solution (Fig. 2b), and no significant difference between AChE$^{+/+}$ and AChE$^{-/-}$ mice was observed (Fig. 5a, left). MEPP amplitudes recorded during the first 100 ms after the train were unaltered in AChE$^{+/+}$

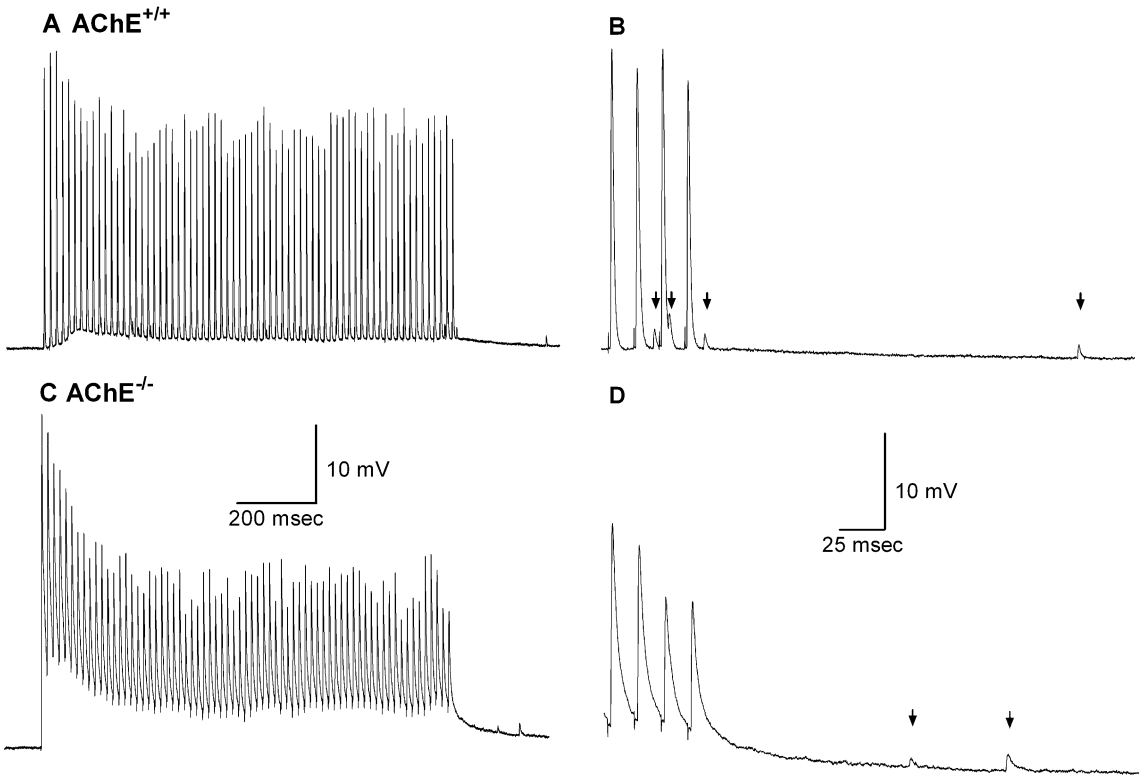

Fig. 4 EPPs elicited by repetitive stimulation at 70 Hz in the presence of 2.5 μM μ-CTX in diaphragms from AChE$^{+/+}$ (**a**) or AChE$^{-/-}$ mice (**c**); the last 4 EPPs and post-tetanic MEPPs (*arrows*) are shown on an expanded time base in (**b**) and (**d**). Most muscle fibers from AChE$^{+/+}$ mice and ~60% from AChE$^{-/-}$ mice exhibited facilitation of EPPs during the second or third stimulation. The shift in baseline in (**a**) is likely the consequence of weak contraction of underlying muscle fibers, and was only infrequently observed, whereas that in (**c**) is due primarily to depolarization of the postsynaptic membrane during the high frequency train and was always observed. Trains were elicited for a duration of 1 s at 3-min intervals. Resting potentials were −61 mV in (**a**) and −63 mV in (**c**)

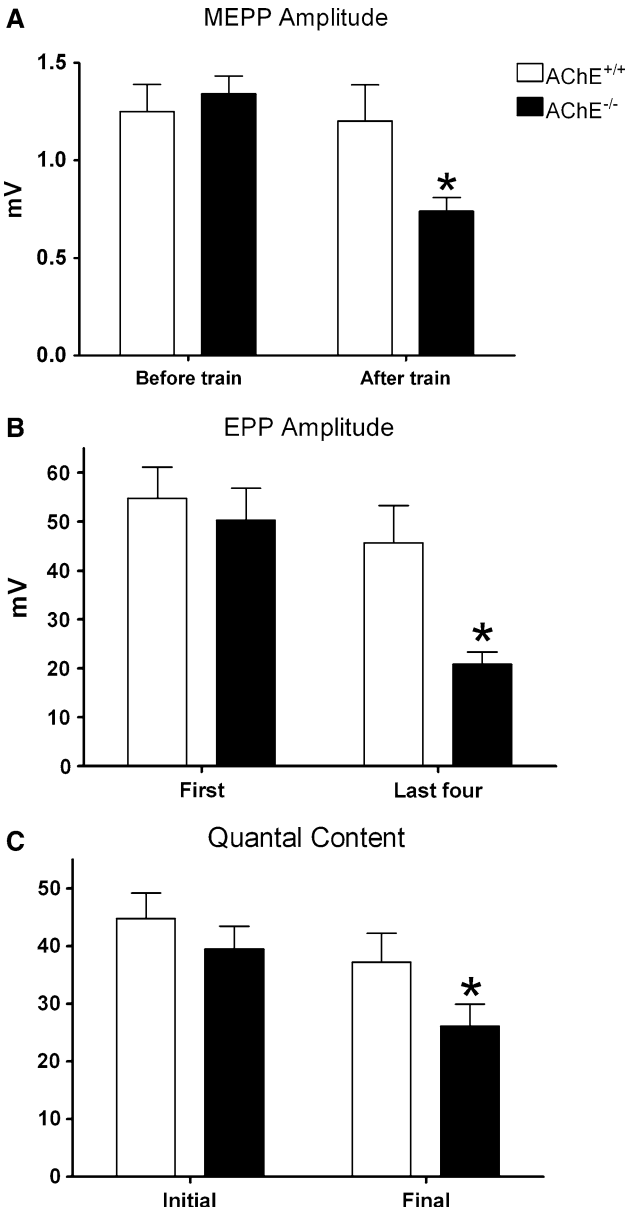

Fig. 5 Histograms of MEPP amplitude (**a**), EPP amplitude (**b**) and quantal content (**c**) obtained prior to, during and following 70 Hz trains (1 s) in muscle fibers from $AChE^{+/+}$ and $AChE^{-/-}$ mice. **a** MEPPs were recorded for a 1-min period prior to stimulation (*Before train*) and for 100 ms after the last EPP (*After train*). **b** Amplitudes of the first EPP and the average of the last four EPPs were determined for each fiber. **c** Quantal content was calculated by the ratio of EPP/MEPP amplitudes. *Initial* was calculated from the first EPP in the train and MEPPs that were recorded during 1 min prior to the train ($m_{r\ Initial}$). *Final* values were obtained from the average of the last four EPP amplitudes divided by MEPP amplitudes recorded for 100 ms after the end of the train ($m_{r\ Final}$). Averaging of four responses served to reduce the effect of random fluctuation in determining the final EPP amplitude. For all histograms, EPPs were corrected for non-linear summation, and MEPPs were referenced to a resting potential of −70 mV. The data represent the mean ± SEM of values from 12 to 16 muscle fibers from at least 3 $AChE^{+/+}$ and 3 $AChE^{-/-}$mice. *Differs significantly from values in corresponding control $AChE^{+/+}$ diaphragm, $P < 0.05$. All recordings were in the presence of 2.5 μM μ-CTX

mice, but underwent a significant reduction in $AChE^{-/-}$ mice of nearly 40% relative to post-tetanic MEPPs in the wild-type mice (Fig. 5a, right, $P \leq 0.05$).

EPP amplitudes determined from the first response in the train showed no alteration between $AChE^{+/+}$ and $AChE^{-/-}$ mice (Fig. 5b, left), whereas amplitudes at the end of the train (average of last four) exhibited a reduction of 59% in $AChE^{-/-}$ mice ($P \leq 0.05$; Fig. 5b, right). From the values of EPPs and MEPPs, we calculated the quantal content of the EPP prior to and following the 70 Hz train. Using the ratio of the first EPP and the mean value of MEPPs obtained during 1-min periods prior to the train, no significant difference in quantal content ($m_{r\ Initial}$) was found between values in $AChE^{+/+}$ and $AChE^{-/-}$ mice (Fig. 5c, left). Using the ratio of the last four EPPs of the train and MEPP amplitudes recorded 100 ms following the train, a 34% reduction in quantal content ($m_{r\ Final}$) was observed ($P \leq 0.05$; Fig. 5c, right).

These data indicate that during high frequency stimulation, a combination of presynaptic (decrease in m_r) and post-synaptic factors (depolarization/desensitization) led to transient reduction of EPP amplitudes. Of importance was the finding that the amplitudes reached a plateau, and did not decline progressively with stimulation (Fig. 4). At the plateau level, it would still be possible to trigger action potentials (in the absence of μ-CTX). The ability of $AChE^{-/-}$ diaphragm muscle to maintain firing arises from the high safety factor of neuromuscular transmission, such that EPPs need only reach a potential of approx. −55 mV to achieve threshold for spike generation.

Synaptic Ultrastructure

To investigate morphological alterations of endplates resulting from the absence of AChE, we examined neuromuscular junctions of $AChE^{+/+}$ and $AChE^{-/-}$ hemidiaphragms by TEM. Typical neuromuscular junctions from an $AChE^{+/+}$ mouse and an age-matched $AChE^{-/-}$ mouse are shown in Fig. 6a and b, respectively. Neuromuscular junctions from $AChE^{-/-}$ mice displayed marked abnormalities, including alterations of presynaptic membranes, synaptic clefts and junctional folds (Fig. 6b). Nerve terminals exhibited a smaller surface area and appeared to contain fewer SSVs. Junctional folds were reduced in number and irregular in shape. In addition, Schwann cells, which are normally found on the outer surface of the nerve terminal, were often observed extending into the synaptic cleft. This is clearly illustrated in the inset to Fig. 6b, where a Schwann cell process is positioned between the nerve terminal and the primary synaptic cleft, and in the upper right section of Fig. 6b, where a nerve terminal is completely engulfed by a Schwann cell.

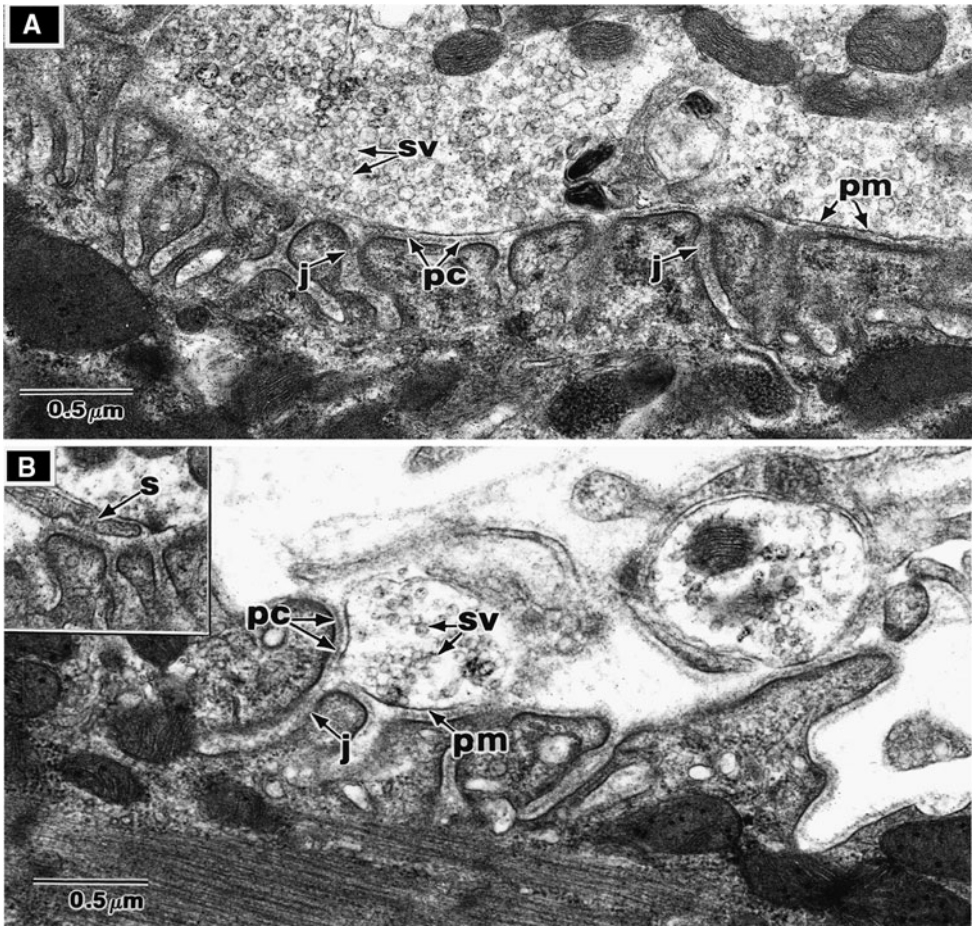

Fig. 6 **a** Motor endplate from a diaphragm muscle of an $AChE^{+/+}$ mouse. Structures indicated are synaptic vesicles (sv), presynaptic membrane (pm), primary cleft (pc) and junctional folds (j). **b** Motor endplate from a diaphragm of an $AChE^{-/-}$ mouse. Note Schwann cell process (s) occupying the primary cleft. *Inset* 37,000×. Endplates shown here are representative of over 106 examined. $AChE^{+/+}$ and $AChE^{-/-}$mice were from the same age group as those used in the electrophysiological study

The cumulative effect of these alterations would result in reduction of pre- and post-synaptic contacts and the opening of additional pathways for diffusion of ACh. These findings are consistent with morphological changes described in patients with a genetic impairment of collagen-tailed AChE (Hutchinson et al. 1993). Significantly, $AChE^{-/-}$ endplates did not show swelling of organelles (mitochondria, endoplasmic reticulum) or supercontractions, which are common ultrastructural changes following acute inhibition of AChE (Laskowski et al. 1977; Adler et al. 1992).

Discussion

The present study was undertaken to determine the characteristics of neuromuscular physiology and ultrastructure in $AChE^{-/-}$ mice. Examination of muscle contractility revealed that $AChE^{-/-}$ mice were able to generate sustained neurally elicited tetanic tensions at 70 and 100 Hz, but produced decremental responses at lower and higher stimulation frequencies (Fig. 1). These findings suggest that AChE KO mice had adapted to the absence of AChE, since acute inhibition of AChE leads to a pronounced tetanic fade, which becomes more severe with increases in stimulation frequency (Heffron and Hobbiger 1979; Adler et al. 2004).

An important adaptation that we identified in a previous study was a reduction in AChR density at the $AChE^{-/-}$ endplate (Adler et al. 2004). Reduction of AChRs would have the effect of accelerating the removal of ACh by diffusion, since the high density of receptors at the endplate acts to retard the efflux of ACh from the synaptic cleft (Katz and Miledi 1973; Magleby and Pallotta 1981). Since downregulation of nicotinic AChRs has also been reported to be triggered by chronic exposure to cholinesterase inhibitors (Costa and Murphy 1983), the loss of AChRs is likely to be a consequence of ACh accumulation. Moreover, Hutchinson et al. (1993) have found similar reductions in AChRs in muscles from patients with congenital human AChE collagen tail deficiency.

Our current TEM study suggests that there is also a reduction in the fraction of the post-junctional membrane that is in contact with the nerve terminal and an overall simplification of the junctional folds (Fig. 6b). It has been estimated that the normal junctional folds, such as those

illustrated in Fig. 6a, increase the AChR-containing post-synaptic membrane surface by a factor of 5 (Wood and Slater 1997). Accordingly, the modified junctional folds of AChE$^{-/-}$ mice would act to reduce the post-junctional surface area and contribute to the lower density of AChRs.

An additional alteration that was prominent in AChE$^{-/-}$ mouse endplates was a marked reduction in nerve terminal size (Fig. 6). Terminals appeared to become fragmented such that each presented a smaller region of contact with post-junctional membranes. In many AChE$^{-/-}$ endplates, the contact area between pre- and post-synaptic membranes was diminished further by insertion of Schwann cell extensions into the synaptic space (Fig. 6b, inset). Since a nerve terminal that extends over the entire synaptic space acts as a physical barrier to the diffusion of ACh, the presence of fragmented terminals would increase diffusion by creating more pathways for the elimination of ACh (Katz and Miledi 1973). The increased diffusion of ACh would in turn lead to a lower level of receptor desensitization. The presence of more numerous terminals ensures that the release of ACh would not be diminished and may account for the finding that quantal content was in the normal range in endplates of AChE KO mice except during high frequency stimulation (Figs. 3, 5).

The electrophysiological and morphological alterations observed in AChE$^{-/-}$ mice differ markedly from those reported following acute AChE inhibition. The latter results in striking increases in the amplitude and decay of EPPs and MEPPs (Katz and Miledi 1973). This contrasts with the less pronounced increase in MEPP decay times and the absence of change in their peak amplitude that was observed in the present study (Figs. 2, 5). Moreover, acute inhibition of AChE produces a focal lesion in the immediate vicinity of the endplate that is characterized by supercontractions and by the swelling of mitochondrial and endoplasmic reticular membranes (Laskowski et al. 1977; Adler et al. 1992). These were not observed in the present study (Fig. 6). The absence of increases in the MEPP amplitude, or of organelle damage, suggests that ACh accumulation is less extensive in AChE$^{-/-}$ muscle than in wild-type muscle in which AChE is acutely inhibited.

In addition to the morphological alterations described above, it is possible that BChE activity also contributes to the maintenance of neuromuscular function. A possible role for BChE is suggested by its apparent synaptic localization (Minic et al. 2003; Girard et al. 2007), and by the finding that the selective BChE inhibitor iso-OMPA enhanced tetanic fade in AChE$^{-/-}$ muscle (Adler et al. 2004). A contribution by BChE activity does not appear to be the case for quantal responses, since iso-OMPA failed to alter MEPPs in either wild-type or AChE-KO mice (Fig. 2). BChE is more likely to play a role during high frequency repetitive stimulation when ACh concentrations are elevated and more sustained (Heffron and Hobbiger 1979; Magleby and Pallotta 1981; Adler et al. 2004; Girard et al. 2007).

Reductions in nicotinic AChR density and alterations of synaptic morphology appear to be the principal adaptive responses to chronic excess ACh, and both are suggested to facilitate the diffusion of ACh out of the synaptic cleft. BChE serves to hydrolyze ACh during high frequency stimulation, but does not contribute to the removal of ACh after release of single ACh quanta. This is consistent with reports that BChE activity does not increase in AChE$^{-/-}$ mice, but rather, this enzyme assumes a latent function that was originally carried out by AChE (Li et al. 2000). The above conclusion is supported by the finding that selective inhibition of BChE is lethal in AChE$^{-/-}$ mice, but is without effect in wild-type littermates (Xie et al. 2000).

The lack of change in MEPP amplitude in AChE$^{-/-}$ mice (Figs. 2, 5) suggests that there is no reduction in the ACh content of the SSV. Other possible adaptations such as a reduction in the number of quanta released per impulse or a reduction in the desensitization rate of AChRs, which are potentially adaptive, do not seem to occur (Hutchinson et al. 1993; Minic et al. 2003; Adler et al. 2004; Girard et al. 2007). Since alterations in AChR density and synaptic morphology take time to develop, these adaptations are not possible during acute AChE inhibition, making this condition rapidly fatal.

One of the more striking features of neuromuscular transmission in AChE$^{-/-}$ mice is the ability of diaphragm muscles to maintain tension at 70 and 100 Hz, whereas tensions at lower or higher frequencies decremented with time (Fig. 1). To shed light on this phenomenon, we examined neuromuscular transmission at 70 Hz in the presence of μ-CTX. Of considerable interest was the finding that based on the first response in the train, EPP and MEPP amplitudes and quantal contents were in the control range (Figs. 4, 5). This suggests that the compensatory mechanisms are able to maintain a functional neuromuscular synapse, in spite of multiple abnormalities in synaptic structure and function. However, consistent with the impaired ability of these preparations to eliminate ACh, consecutive EPPs were observed to decrement with time (Fig. 4). In spite of this decrement, stabilization of EPP amplitudes during the latter part of the train (Fig. 4) in conjunction with the relatively long duration of single twitches (Table 1) and their larger amplitudes (Fig. 1) allowed for maintained tetanic tension in the diaphragm muscle at a level adequate for survival.

Comparison of Figs. 1 and 4 reveals an overall similarity in the configuration of EPPs and muscle tensions at 70 Hz. Maximal tetanic tension was reached early during stimulation, and corresponded to the fusion of two individual twitches at their peak values. Subsequently, the

70-Hz tetanus underwent a transient fall, triggered by the corresponding fall in the EPP amplitudes from depolarization and subsequent desensitization of the postjunctional membrane and transient depletion of the immediately releasable pool of SSVs (Elmqvist and Quastel 1965). Subsequently, the EPP amplitudes reached a plateau which is reflected in the plateau of the tetanic tension profile.

Based on the forgoing, the tetanic fade observed at 50 Hz may seem somewhat surprising since desensitization is known to be frequency-dependent (Magleby and Pallotta 1981). However, with a peak contraction time of 15.9 ms for the single twitch (Table 1), the interval between pulses at 50 Hz (20 ms) leads to summation of tetanic responses on the relaxation phase of the twitches, rather than at their peaks, which presumably accounts for the more intense tetanic fade at 50 Hz. Using the same argument, the superior tetanic tension profile at 70 or 100 Hz (pulse interval of 14.3 or 10 ms, respectively) may be the result of the improved tetanic summation, while the pronounced tetanic fade at 200 Hz would reflect collapse of the compensatory mechanisms.

Acknowledgments We dedicate this article to the memory of Dr. Marshall Nirenberg, in whose laboratory the primary author (MA) had the privilege of working from 1978 to 1982. Dr. Nirenberg was a strong proponent of using genetic tools for solving problems in neurobiology and for tackling important scientific issues regardless of their complexity. This research was supported by the Defense Threat Reduction Agency—Joint Science and Technology Office, Medical S&T Division. The opinions or assertions contained herein are the private views of the authors and are not to be construed as official or as reflecting the views of the Army or the Department of Defense. In conducting the research described in this report, the investigators complied with the regulations and standards of the Animal Welfare Act and adhered to the principles of the Guide for the Care and Use of Laboratory Animals (http://www.nap.edu/catalog.php?record_id=12910).

References

Adler M, Petrali JP, Moore DH, Filbert MG (1991) Function and distribution of acetyl- and butyrylcholinesterase in canine tracheal smooth muscle. Arch Int Pharmacodyn Ther 312:126–139

Adler M, Hinman D, Hudson CS (1992) Role of muscle fasciculations in the generation of myopathies in mammalian skeletal muscle. Brain Res Bull 29:179–187

Adler M, Manley HA, Purcell A, Deshpande SS, Hamilton TA, Kan RK, Oyler G, Lockridge O, Duysen EG, Sheridan RE (2004) Reduced acetylcholinesterase receptor density, morphological remodeling, and butyrylcholinesterase activity can sustain muscle function in acetylcholinesterase knockout mice. Muscle Nerve 30:317–327

Akk G, Milescu LS, Heckmann M (2005) Activation of heteroliganded mouse muscle nicotinic receptors. J Physiol 564:359–376

Albuquerque EX, Pereira EF, Aracava Y, Fawcett WP, Oliveira M, Randall WR, Hamilton TA, Kan RK, Romano JA Jr, Adler M (2006) Effective countermeasure against poisoning by organophosphorus insecticides and nerve agents. Proc Natl Acad Sci USA 103:13220–13225

Bois RT, Hummel RG, Dettbarn W-D, Laskowski M (1980) Presynaptic and Postsynaptic neuromuscular effects of a specific inhibitor of acetylcholinesterase. J Pharmacol Exp Ther 215:53–59

Brimijoin S, Koenigsberger C (1999) Cholinesterases in neural development: new findings and toxicologic implications. Environ Health Perspect 107(Suppl 1):59–64

Chatonnet A, Lockridge O (1989) Comparison of butyrylcholinesterase and acetylcholinesterase. Biochem J 260:625–634

Colletier JP, Fournier D, Greenblatt HM, Stojan J, Sussman JL, Zaccai G, Silman I, Weik M (2006) Structural insights into substrate traffic and inhibition in acetylcholinesterase. EMBO J 25:2746–2756

Costa LG, Murphy SD (1983) [^{3}H]Nicotine binding in rat brain: alteration after chronic acetylcholinesterase inhibition. J Pharmacol Exp Ther 226:392–397

Del Castillo J, Katz B (1954) Quantal components of the end-plate potential. J Physiol (Lond) 124:560–573

Duysen EG, Li B, Xie W, Schopfer LM, Anderson RS, Broomfield CA, Lockridge O (2001) Evidence for nonacetylcholinesterase targets of organophosphorus nerve agent: supersensitivity of acetylcholinesterase knockout mouse to VX lethality. J Pharmacol Exp Ther 299:528–535

Duysen EG, Stribley JA, Fry DL, Hinrichs SH, Lockridge O (2002) Rescue of the acetylcholinesterase knockout mouse by feeding a liquid diet; phenotype of the adult acetylcholinesterase deficient mouse. Dev Brain Res 137:43–54

Elenes S, Auerbach A (2002) Desensitization of diliganded mouse muscle nicotinic acetylcholine receptor channels. J Physiol (Lond) 541:367–383

Elmqvist D, Quastel DMJ (1965) A quantitative study of endplate potentials in isolated human muscle. J Physiol (Lond) 178:505–529

Fiekers JF (1985) Interactions of edrophonium, physostigmine and methanesulfonyl fluoride with the snake end-plate acetylcholine receptor-channel complex. J Pharmacol Exp Ther 234:539–549

Girard E, Bernard V, Minic J, Chatonnet A, Krejci E, Molgó J (2007) Butyrylcholinesterase and the control of synaptic responses in acetylcholinesterase knockout mice. Life Sci 80:2380–2385

Hartmann J, Kiewert C, Duysen EG, Lockridge O, Greig NH, Klein J (2007) Excessive hippocampal acetylcholine levels in acetylcholinesterase-deficient mice are moderated by butyrylcholinesterase activity. J Neurochem 100:1421–1429

Heffron PF, Hobbiger F (1979) Relationship between inhibition of acetylcholinesterase and response of the rat phrenic nerve-diaphragm preparation to indirect stimulation at higher frequencies. Br J Pharmacol 66:323–329

Heuser JE, Reese TS, Dennis MJ, Jan Y, Jan L, Evans L (1979) Synaptic vesicle exocytosis captured by quick freezing and correlated with quantal transmitter release. J Cell Biol 81:275–300

Hutchinson DO, Walls TJ, Nakano S, Camp S, Taylor P, Harper CM, Groover RV, Peterson HA, Jamieson DG, Engel AG (1993) Congenital endplate acetylcholinesterase deficiency. Brain 116:633–653

Karlin A (2002) Emerging structure of the nicotinic acetylcholine receptors. Nat Rev Neurosci 3:102–114

Katz B, Miledi R (1973) The binding of acetylcholine to receptors and its removal from the synaptic cleft. J Physiol (Lond) 231:549–574

Kuba K, Albuquerque EX, Daly J, Barnard EA (1974) A study of the irreversible cholinesterase inhibitor, diisopropylfluorophosphate, on time course of end-plate currents in frog sartorius muscle. J Pharmacol Exp Ther 189:499–512

Lane RM, Potkin SG, Enz A (2006) Targeting acetylcholinesterase and butyrylcholinesterase in dementia. Int J Neuropsychopharmacol 9:101–124

Laskowski MB, Olsen WH, Dettbarn W-D (1977) Initial ultrastructural abnormalities at the motor end plate produced by a cholinesterase inhibitor. Exp Neurol 57:13–33

Li B, Stribley JA, Ticu A, Xie W, Schopfer LM, Hammond P, Brimijoin S, Hinrichs SH, Lockridge O (2000) Abundant tissue butyrylcholinesterase and its possible function in the acetylcholinesterase knockout mouse. J Neurochem 75:1320–1331

Magleby KL, Pallotta BS (1981) A study of desensitization of acetylcholine receptors using nerve-released transmitter in the frog. J Physiol (Lond) 316:225–250

McLachlan EM, Martin AR (1981) Non-linear summation of endplate potentials in the frog and mouse. J Physiol (Lond) 311: 307–324

Mesulam M, Guillozet A, Shaw P, Quinn B (2002) Widely spread butyrylcholinesterase can hydrolyze acetylcholine in the normal and Alzheimer brain. Neurobiol Dis 9:88–93

Minic J, Chatonnet A, Krejci E, Molgó J (2003) Butyrylcholinesterase and acetylcholinesterase activity and quantal transmitter release at normal and acetylcholinesterase knockout mouse neuromuscular junctions. Br J Pharmacol 138:177–187

Miyazawa A, Fujiyohshi Y, Unwin N (2003) Structure and gating mechanism of the acetylcholine receptor pore. Nature 423:949–955

Mouisel E, Blondet B, Escourrou P, Chatonnet A, Molgó J, Ferry A (2006) Outcome of acetylcholinesterase deficiency for neuromuscular functioning. Neurosci Res 55:389–396

Moyer M, Van Lunteren E (1999) Effect of phasic activation on endplate potential in rat diaphragm. J Neurophysiol 82:3030–3040

Nguyen-Huu T, Molgó J, Servent D, Duvaldestin P (2009) Resistance to d-tubocurarine of the rat diaphragm as compared to limb muscle. Anesthesiology 110:1011–1015

Plomp JJ, Van Kempen GTH, Molenraar PC (1992) Adaptation of quantal content to decreased postsynaptic sensitivity at single endplates in α-bungarotoxin-treated rats. J Physiol (Lond) 458: 487–499

Rosenberry TL, Mallender WD, Thomas PJ, Szegletes T (1999) A steric blockade model for inhibition of acetylcholinesterase by peripheral site ligands and substrate. Chem Biol Interact 119–120:85–97

Taylor PJ (1991) The cholinesterases. J Biol Chem 266:4025–4028

Wood SJ, Slater CR (1997) The contribution of postsynaptic folds to the safety factor for neuromuscular transmission in rat fast- and slow-twitch muscles. J Physiol (Lond) 500:165–176

Xie W, Stribley JA, Chatonnet A, Wilder PJ, Rizzino A, McComb RD, Taylor P, Hinrichs SH, Lockridge O (2000) Postnatal developmental delay and supersensitivity to organophosphate in gene-targeted mice lacking acetylcholinesterase. J Pharmacol Exp Ther 293:896–902

Yu SP, Van der Kloot W (1991) Increasing quantal size at the mouse neuromuscular junction and the role of choline. J Physiol (Lond) 433:677–704

Zimmerman G, Soreq H (2006) Termination and beyond: acetylcholinesterase as a modulator of synaptic transmission. Cell Tissue Res 326:655–969